Highly parallel CMOS lock-in optical sensor array for hyperspectral recording in scanned imaging systems

Roger A. Light*[a], Richard J. Smith[b], Nicholas S. Johnston[a],
Steve D. Sharples[b], Michael G. Somekh[a], Mark C. Pitter[a]
[a]IBIOS, University of Nottingham, University Park, Nottingham, NG7 2RD, UK;
[b]Applied Optics, University of Nottingham, University Park, Nottingham, NG7 2RD, UK

ABSTRACT

Many optical measurements that are subject to high levels of background illumination rely on phase sensitive lock-in detection to extract the useful signal. If modulation is applied to the portion of the signal that contains information, lock-in detection can perform very narrowband (and hence low noise) detection at frequencies well away from noise sources such as 1/f and instrumental drift. Lock-in detection is therefore used in many optical imaging and measurement techniques, including optical coherence tomography, heterodyne interferometry, optoacoustic tomography and a range of pump-probe techniques. Phase sensitive imaging is generally performed sequentially with a single photodetector and a lock-in amplifier. However, this approach severely limits the rate of multi-dimensional image acquisition. We present a novel linear array chip that can perform phase sensitive, shot-noise limited optical detection in up to 256 parallel channels. This has been achieved by employing four independent wells in each pixel, and massively enhancing the intrinsic well depth to suppress the effect of optical shot noise. Thus the array can reduce the number of dimensions that need to be sequentially scanned and greatly speed up acquisition. Results demonstrating spatial and spectral parallelism in pump-probe experiments are presented where the a.c. amplitude to background ratio approaches 1 part in one million.

Keywords: CMOS image sensor, active pixel sensor, modulated light, phase stepping, picosecond ultrasound

1. INTRODUCTION

Most commercial cameras are designed for acquiring relatively high contrast images, where the range of expected instantaneous light intensity is a significant proportion of the input range of the camera and dynamic range requirements are modest. Several specialist cameras have been developed for different light regimes, where extended dynamic range is necessary, for instance, extending the input range of cameras by using multiple exposures[1,2], multiple integration wells per pixel for low and high light conditions[3], logarithmic compression of the intensity[4], or a combination of both linear and logarithmic measurements[5]. The resulting high dynamic range cameras are useful where there is a large intra-frame variation in intensity, such as imaging road traffic at night time or in tunnels[2] for example, but are not suited to all applications.

In experiments where the overall light level is low, read-out noise and dark current are the dominant noise sources. In astronomy, detectors are typically cryogenically cooled to reduce thermal induced dark current and the read-out is carried out slowly to reduce noise[6,7]. Fluorescence lifetime imaging is another area where the detected light intensities are very low. In these applications, however, fast data acquisition is necessary. Cameras designed for time resolved single photon counting are now being produced for use in fluorescence imaging and other high speed, very low light applications[8,9].

A third class of applications, and that which concerns us here, is where there is a significant light intensity arriving at the detector but only a small proportion of this is the signal of interest, resulting in extremely low contrast. This is common in pump-probe type experiments, where an intensity modulated pump laser beam induces a small optical effect on a sample that is then measured using a probe beam[10]. In these types of experiment, the signal of interest may be on the order of 10^{-6} of the background illumination, well beyond the dynamic range of even high quality conventional cameras. The high dynamic range cameras already mentioned are not well suited to this type of signal because they are optimized to measure a wide range of signals, not to accurately determine the magnitude of a small change in a large signal.

*roger.light@nottingham.ac.uk; phone 44 115 8468848; fax 44 115 9515616; nottingham.ac.uk/ibios

The conventional approach to the problem of very low contrast is to modulate the signal portion of the detected intensity and perform lock-in detection with a single photodiode. This setup provides a number of advantages. The discrete photodetector can be of large area and high quality, the system operates in continuous time mode so that as much of the available light is used as possible and the modulation causes the signal of interest to be shifted in the frequency domain so that it is centered at the modulation frequency rather than at d.c. and is away from low frequency noise. The lock-in amplifier operates as a high quality band-pass filter at the modulation frequency and so further reduces the noise in the measurement. Imaging in this way is slow because the illumination or the photodetector must be mechanically scanned in two dimensions. Using multiple detectors quickly becomes impractical and expensive because each detector requires its own lock-in amplifier.

The lock-in amplifier works on the continuous time signal. A number of approaches have been proposed to build the demodulation into individual pixels of a camera,[11-16] but the simplest method is a technique known as phase stepping. A camera capable of operating as a lock-in is known as a modulated light camera. The signal shown in Fig. 1 represents the intensity measured at the detector when the experiment input is modulated. The signal of interest is contained in either the phase or the amplitude, depending on the experiment.

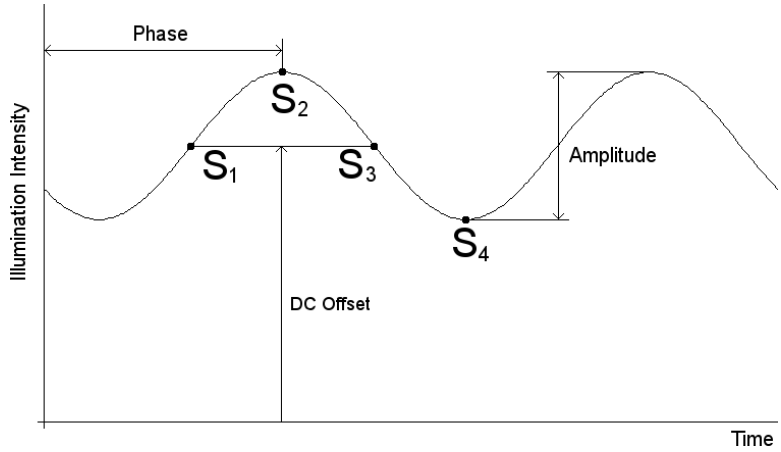

Figure 1. Modulated photocurrent at detector showing signal parameters and sampling points.

This signal has three unknowns, the d.c. offset (B), amplitude (A) and phase (φ). This means that it can be reconstructed using a minimum of three samples. Using four samples as below leads to a more robust measurement and is straightforward to implement in practice. In this case, the samples S_1 to S_4 are acquired at 90 degree intervals as follows:

$$S_1 = B + A\sin(\phi + 0) = B + A\sin(\phi) \tag{1}$$

$$S_2 = B + A\sin(\phi + 90) = B + A\cos(\phi) \tag{2}$$

$$S_3 = B + A\sin(\phi + 180) = B - A\sin(\phi) \tag{3}$$

$$S_4 = B + A\sin(\phi + 270) = B - A\cos(\phi) \tag{4}$$

Equations 1-4 can be used to calculate the d.c., amplitude and phase as follows:

$$B = \frac{S_1 + S_2 + S_3 + S_4}{4} \tag{5}$$

$$A = \frac{\sqrt{(S_1 - S_3)^2 + (S_2 - S_4)^2}}{2} \tag{6}$$

$$\phi = \tan^{-1}\frac{S_1 - S_3}{S_2 - S_4} \tag{7}$$

We can thus simulate lock-in behavior by acquiring four images evenly spaced in time throughout each cycle.

Although a camera capable of a precisely timed high frame rate can be used as a modulated light camera, further improvements over conventional designs are needed to deal with the very low contrast associated with pump-probe and similar experiments. Unlike low light level experiments, the limiting factor here is optical shot noise. For a measurement that utilizes N photons, the shot noise and therefore the signal to noise ratio is $\sqrt{N}$. This imposes strict requirements on the photon budget. For the case of the signal being 10^{-6} of the DC, this means that at least 10^{12} photons must be collected. Using a typical camera pixel able to collect 100 ke^- per frame this would take 10 million frames to achieve.

For both CCD and CMOS sensors, the pixel design most commonly used makes use of the capacitance of the photodetector as a well for storing charge. For CMOS, when the sensor is reset before an image is taken, all of the wells are filled. As the exposure takes place the photocurrent gradually empties the wells at a rate proportional to the illumination intensity. The capacitance of the detector determines the conversion gain, or the rate of change in voltage with integrated photocurrent. Consumer devices tend to have a small well so that relatively few photons cause a measurable change in output voltage. This makes them sensitive to light, but limits their shot noise performance. A device with well depth of 30 ke^- has a maximum signal to noise ratio of 173, or just over 7.4 bits, assuming that it is shot noise limited. Typical scientific cameras have a well depth of a few tens to a few hundred thousand electrons.

2. CAMERA DESIGN AND OPERATION

The custom sensor consists of a linear (1-dimensional) array of 256 pixels fabricated in the Austriamicrosystems C35B4C3 process, a 0.35 μm 2-poly, 4-metal, 3.3 V standard CMOS process.

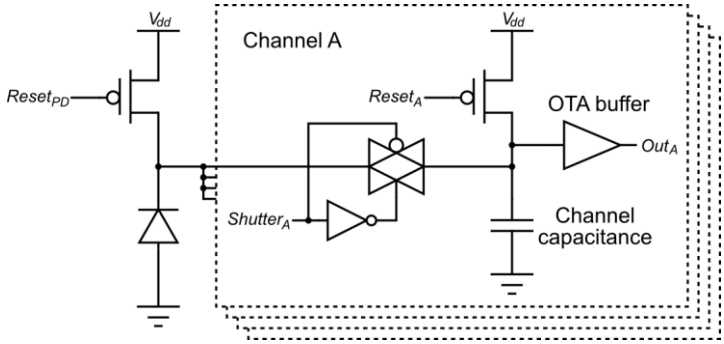

Figure 2. Four channel pixel schematic.

2.1 Pixel design

The pixel design is based on the standard four transistor active pixel sensor (APS), but with four channels instead of a one to allow for demodulation (Fig. 2). Each channel has its own shutter switch, and can either be operated independently or in tandem with others. The shutter is implemented with a transmission gate rather than with an NMOS transistor which increases the dynamic range. Each channel also contains a reset switch and a large supplementary capacitance, henceforth called the channel capacitance, to boost the overall well depth. The channel reset switch can be used to reset the associated channel without its shutter switch needing to be closed. This means that one channel can be reset when another is being exposed, for example. It also provides a dedicated path for the reset current to each channel to flow through, which is important because of the high peak current flow that can occur during reset. The channel capacitance is formed from the gate capacitance of NMOS transistors. The capacitance per unit area of a MOS gate is the highest available on chip and is approximately five times higher than the poly-poly capacitors otherwise used. The disadvantage of using the gate capacitance is that the capacitance value varies with voltage beneath approximately a threshold voltage above ground. The channel capacitance is much larger than that of the photodiode which helps linearize the overall pixel response because the photodiode capacitance has fairly strong voltage dependence across the

whole voltage range. The pixel size is 480 x 25 μm, with the photodiode itself being 480 x 22 μm for a fill factor of 88%. This size leads to a photodiode capacitance of 1.2 pF for a reverse bias voltage of 1.65 V, or half of the positive voltage supply. Each channel capacitance and associated circuitry occupies an area of 714 x 25 μm and has a capacitance of 34.1 pF. They are arranged with two channels on each of the ends of the pixels as shown in Fig. 3.

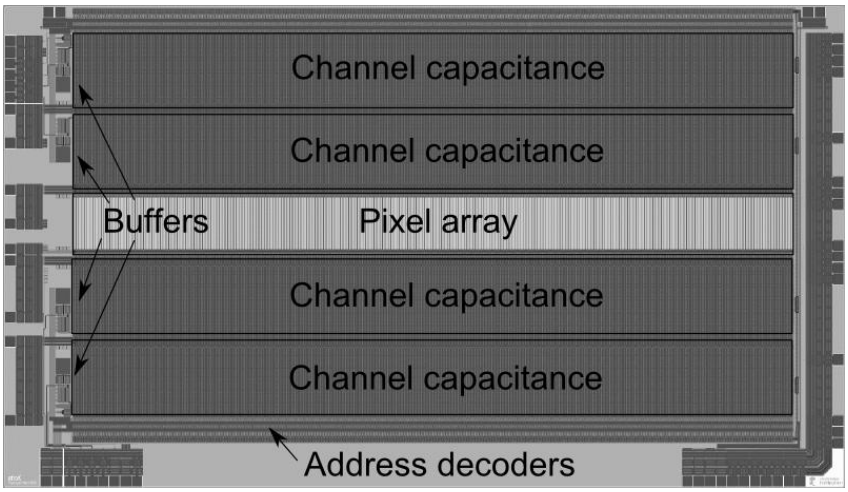

Figure 3. Chip layout.

The output of each channel is buffered by an operational transimpedance amplifier (OTA) configured as a voltage follower to give unity gain. This is another departure from the traditional APS design, where source followers are used. This is made possible by the reduced space restriction due to designing a linear array rather than a 2D array. Using an OTA here gives a much more linear response than a source follower and doesn't introduce a d.c. offset onto the output which helps maximize the dynamic range. The OTA has been implemented using 5 V tolerant transistors rather than the usual 3.3 V transistors for this process, and it is powered by a 5 V supply rail. Because the input will never rise above 3.3 V, this gives a simple way of producing an amplifier with linear response up to the positive input and output rail. The OTA response does become non-linear when the input is close to a threshold voltage above ground but this is of much less concern because the capacitance of the channel capacitor also begins to change at this point, which would lead to a non-linear output even with an ideal OTA.

2.2 Chip buffers

The output of the OTA for each channel is passed through a 256:1 multiplexer and through a further buffer (the chip buffer), from where it is sent off chip. This results in four chip buffers, allowing all four channels of a single pixel to be read in parallel. Like the OTAs, the operational amplifier design for the chip buffers is implemented using 5 V tolerant transistors to give improved headroom. The chip buffers have a -3 dB small signal bandwidth of 170 MHz and a slew rate of 10 V/μs, meaning that a pixel rate in excess of 10 MHz should be easily achievable, assuming that the variation in recorded pixel to pixel voltage does not exceed 1 V. This equates to a maximum demodulated frame rate of just below 40 kHz, where a demodulated frame is the calculated result from the four channel image using equation 6.

2.3 Pixel variable gain

The channel capacitance actually consists of eleven nominally identical 3.1 pF capacitors connected in parallel. The schematic for one of these sub-capacitors is shown in Fig. 4. The sub-capacitors are each connected in series with a transmission gate which can be turned on and off to connect and disconnect each sub-capacitor to one another, thus changing the well depth of the channel. The latch is used to store the switch value in a permanent state.

This means that the effective well depth can be expressed as shown in equation 8, where n is the number of sub-capacitors connected together ($n > 0$):

$$W_{e^-} = 20.3\text{Me}^- + n*52.3\text{Me}^- \quad (8)$$

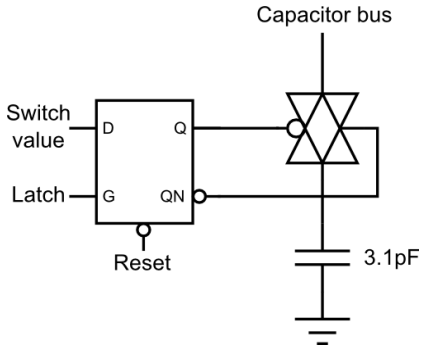

Figure 4. Sub-capacitor schematic, of which eleven are connected in parallel per pixel channel.

Each individual pixel within the array can be programmed with its own well depth. This has important implications for applications where there is non-uniformity in the illumination intensity distribution across the camera that is caused by the optical input to the experiment, rather than the experiment itself.

2.4 Theoretical noise performance

A single channel capacitance is 34.1 pF which gives a maximum well depth of 730 Me^- per channel, including the photodiode capacitance, over the full 3.3 V voltage range. The maximum practical range is less than this because of the non-linearity of the OTA buffer and channel capacitance itself at low voltages. A reasonable working range is 0.6-3.3 V, or a swing of 2.7 V, giving an effective well depth of 600 Me^- per channel including the photodiode capacitance. At this well depth, the shot noise is 24.5 ke^-. This means for a signal to background ratio of $1{:}10^4$ only a single measurement is required, for $1{:}10^5$ just 5 demodulated frames are required and for $1{:}10^6$, 420 demodulated frames are required.

The noise calculations considered so far have assumed the best case where the noise is dominated by shot noise. Other important sources of noise in imagers are read out noise and reset noise. We have performed noise simulations with the Cadence Spectre simulator to determine the expected noise from the pixel to the output at the pad. In a bandwidth of 500 kHz, the sample rate of our current acquisition system, the total integrated read noise is 34.1 μV. This equates to 7.5 ke^- for a full well, which means that the shot noise and the read noise will be equal when the well is filled to 56.3 Me^- or just less than 10% of the effective well depth. Reset noise is the thermal noise present on the integration capacitance in the pixel during reset and is calculated as $\sqrt{kT/C}$ (volts), where k is Boltzmann's constant, T is temperature in kelvin and C is the integration capacitance in farads. At room temperature this gives a reset noise of 11 μV or 2.4 ke^-. The read noise and reset noise are uncorrelated, so they add in quadrature to give a total noise of 7.9 ke^- and so the pixel should be shot noise limited for over 90% of its useful range.

Although measurements will remain shot noise limited for a wide range of input illuminations, they can be further improved. If the intensity on one pixel is half that of another pixel, it is likely that the signal of interest on the second pixel will be proportionally smaller. This makes measurement more difficult because the change in voltage at the output will also be twice as small. By using the variable gain to halve the well depth in this case, both pixels will in theory produce a similar change in voltage, assuming there are no other differences in the signals. Using the full voltage range makes full use of the dynamic range of the acquisition system. Most importantly, the read out noise is essentially a fixed voltage level regardless of illumination or well depth, so extending the voltage range diminishes the effect of the read out noise.

Considering the case where only a single sub-capacitor is used, the per-channel capacitance is 4.3 pF. This gives a maximum effective well depth of 73 Me^- and 8.5 ke^- of shot noise. The 34.1 μV read out noise is now equivalent to 916 e^- and the reset noise at room temperature is 31 μV or 834 e^-. The combined total of the read out and reset noise is 1.2 ke^- so a pixel in this configuration should remain shot noise limited down to 1.5 Me^- well in use.

Another source of error in imagers is dark current, which is current that flows in the photodetector that is due to thermally generated carriers or other forms of leakage not related to the illumination. This is especially important in this variable gain sensor because the dark current will remain unaffected by the variable well depth; the voltage offset caused by the dark current will increase as the well depth is set to a lower value. The effect of this variable offset can be removed by taking a number of dark images just prior to the experiment. By using the same gain and exposure settings for the dark images as for the actual experiment, the correct amount of offset will be removed.

2.5 Operation

The sensor offers flexibility in its operation to suit a range of experiments. In addition to the modulated detection described in this paper, it may be used in any application that requires a high degree of temporal resolution.

When being used as a modulated light camera, the operation depends on the relationship between the modulation frequency and the sampling frequency. If the sampling frequency is high enough to acquire 256 samples within a quarter of the modulation period, then it is possible to simultaneously sample one channel whilst another channel is being exposed. This arrangement makes the most efficient use of the available light. The photodiodes are reset for 1 μs between each exposure, so for a 10 kHz modulation frequency the camera will be in carrying out an exposure for 99.9% of the modulation period, but would require a sampling frequency of 10 MHz. Our current acquisition system has a maximum sampling frequency of 500 kHz and so has a maximum modulation frequency of approximately 480 Hz.

If the acquisition speed is insufficient to meet this demand then a different scheme may be used by taking the exposures for all four channels in order and only then carrying out the acquisition. This scheme removes the need for high speed acquisition because the sampling is decoupled from the exposure. It allows the use of parallel acquisition systems because all four channels are being sampled at once and makes possible the partial solving of equations 5 and 6 by calculating $S_1 - S_3$ and $S_2 - S_4$ using analog electronics. The disadvantage is that the light usage is much less efficient. For a modulation frequency of 10 kHz and a sampling frequency of 10 MHz the camera will be exposing for 48% of the overall frame time. With a sampling frequency of 500 kHz this drops to 4.5% of the frame time.

3. OPTICAL SETUP

We present results from a picosecond ultrasonic experiment[14]. The experimental arrangement is shown in Fig. 5, where the output from a short pulse width laser (spectra physics Tsunami, 100 fs pulse width, 80 MHz repetition rate, 800 nm wavelength) is split into two beams. One beam, the pump, is modulated by a mechanical chopper at a low frequency for lock-in detection and is focused to a ~3 μm spot onto the sample by a 0.6 NA objective lens. When the pump pulse energy is absorbed by the sample it creates an area of rapid local heating and therefore thermal expansion. This expansion launches an acoustic wave packet into the sample. The probe beam is focused to the same location on the sample as the pump beam. The time at which the probe beam arrives and therefore the time it interacts with the propagating sound wave is controlled by changing the length of the optical delay line. On reflection from the sample the probe beam is dispersed by a grating and the first order is focused onto the array by a lens so that each pixel measures the response for a different probe wavelength.

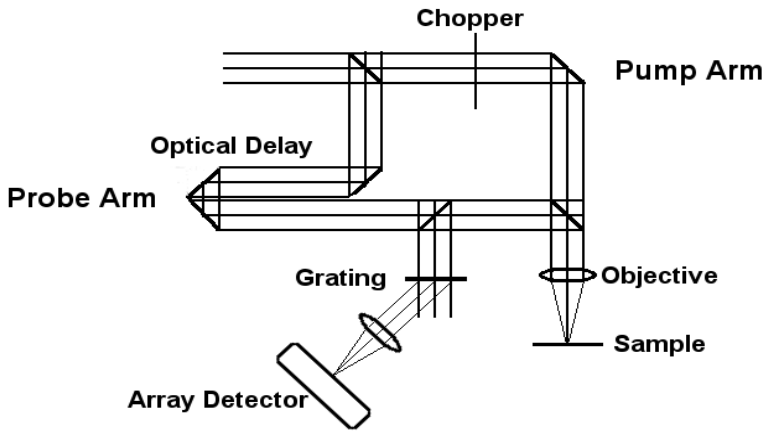

Figure 5. Optical arrangement

The sample used in this example is GaAs <111> and as this is semi-transparent for the range of wavelengths used, the change in the reflectivity of the probe beam is oscillatory in nature. This is because the sample forms an interferometer where one part of the probe beam is reflected from the sample/air interface and another part is reflected from the

propagating acoustic wave. As time passes the acoustic wave travels further into the sample and this causes the phase of the acoustically reflected component to change, leading to an oscillating signal termed Brillouin oscillations[15].

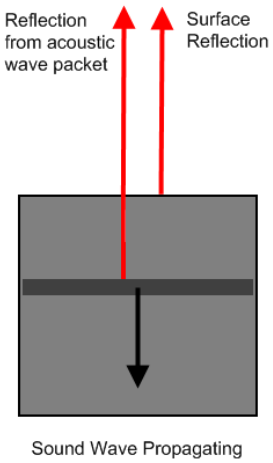

Figure 6. Detection of Brillouin oscillations on GaAs <111>

The frequency of the oscillations is given by equation 9 below, where, *n* is the real part of the refractive index (~3.7), *Va* is the acoustic velocity (~5400 m/s), λ is the wavelength (~800-815 nm) and θ is the angle of incidence of the probe beam which is usually zero in our case. As can be seen, the recorded frequency is dependent on the acoustic velocity and the probe wavelength within the sample.

$$f_b = \frac{2v_a n}{\lambda}\cos\vartheta \tag{9}$$

The returning acoustic wave induces stress in the material which produces a small change (1 part in 10^5 or 10^6) in the reflectivity of the sample. This change is detected by chopping the pump beam so the probe beam reflectivity is switched between the reflectivity with and without the pump beam. This small fluctuation on a large constant background carries the information of the propagating ultrasonic wave. In a conventional system this is detected with a photodiode and lock-in amplifier, here we replace this single point measurement with the linear camera chip described above.

The grating is used to disperse the different wavelengths from the *fs* laser pulse and each pixel of the detector measures a different oscillation frequency, as predicted from equation 9. We are thus able to record the interaction between the probe beam and different acoustic frequencies within the sample in a single parallel measurement.

4. RESULTS

4.1 Dark noise performance

An initial noise characterization has carried out by taking measurements of the camera operating in the dark. This allows a measure of the read out noise to be calculated. The measurements were made with a National Instruments PCI-6281, an 18-bit, 500 ksps acquisition card. 1500 frames were acquired in exactly the same manner as when the camera is normally in use, with a sampling frequency of 500 ksps and a modulation frequency of 450 Hz, for an exposure time per channel of 8.9 ms. The standard deviation of the acquisitions was calculated for each pixel and channel. The mean of these values was calculated as 64 µV, with a pixel to pixel standard deviation of 1.2 µV. This allows the region over which the camera is shot noise limited to be recalculated. When operating with all eleven sub-capacitors in use, the read noise of 64 µV is equivalent to 14.12 ke^-, meaning that the camera should be shot noise limited if more than 200 Me^- electrons are collected, or at least 33% of the effective well depth. When only a single sub-capacitor is in use, the read noise is equivalent to 1.8 ke^-, making the camera shot noise limited for 3.2 Me^- and above, or over 95% of the effective well capacity.

4.2 Spectroscopic measurements

The signals obtained from this type of experiment usually have three main components, a step change in the response at time t=0 where the pump and probe beams are temporally aligned (coincident peak), a slow thermal relaxation curve and superimposed on this is the oscillating signal of interest. Figure 7 shows the demodulated output from the detector after the thermal background was removed by subtracting a low order polynomial curve.

In this case 200 averages were used, and the light was dispersed across the detector with a 1200 line/mm grating and focused onto the detector by a lens with focal length of 100 mm. Each pixel therefore corresponds to a change in probe wavelength of ~0.06 nm, giving a total optical bandwidth across the detector of ~16 nm.

The measured oscillations are well defined and the signals are visible over most of the detector pixels. The modulation depth of the recovered signals is ~$0.5\text{x}10^{-4}$ → $1\text{x}10^{-5}$ with respect to the d.c. light level.

The frequency of the oscillations for each pixel is shown at the top of Fig. 7. The frequency is changing across the array as expected from equation 9. The measurement of the frequency becomes noisy at the edges of the detector as there is only a small amount of light falling onto these pixels.

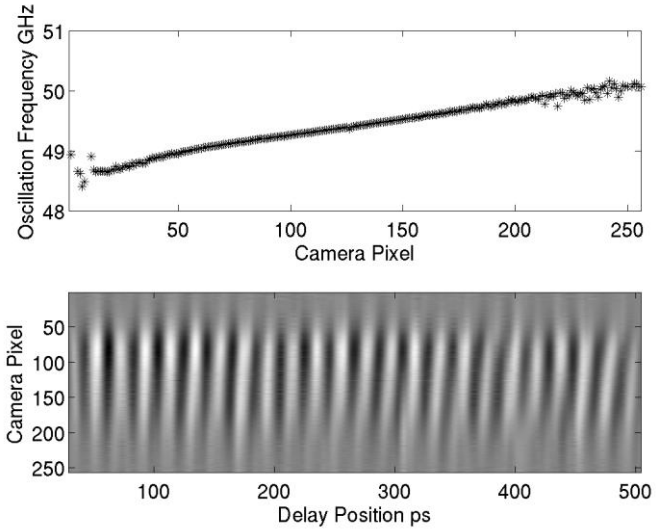

Figure 7. Top: oscillation frequency Bottom: demodulated signal recorded by the detector

To help with the SNR the detector gains can be set for each pixel to increase the signal level. Figure 8 shows the d.c. light distribution where the gains are all the same (solid curve), where the edges have increased gain (dashed) and the gain profile (stepped line). By boosting the signal level of the low light pixels we reduce the influence of readout noise on these signals as discussed in section 2.4.

5. CONCLUSIONS

A 256 pixel linear sensor has been presented. Each pixel has four independent very large wells, making the detection of modulated signals in the presence of high background illumination possible. The capability of detecting signals of the order of 10^{-5} of the background illumination level has been demonstrated. The sensor is usable over a range of illuminations and can be tailored to provide the best voltage response to a specific illumination profile through the use of the per-pixel variable gain. The variable gain also extends the range over which the sensor is shot noise limited, from 66% of the effective well depth if only the largest well were available to 95% of the effective well depth when operating at a sampling frequency of 500 kHz.

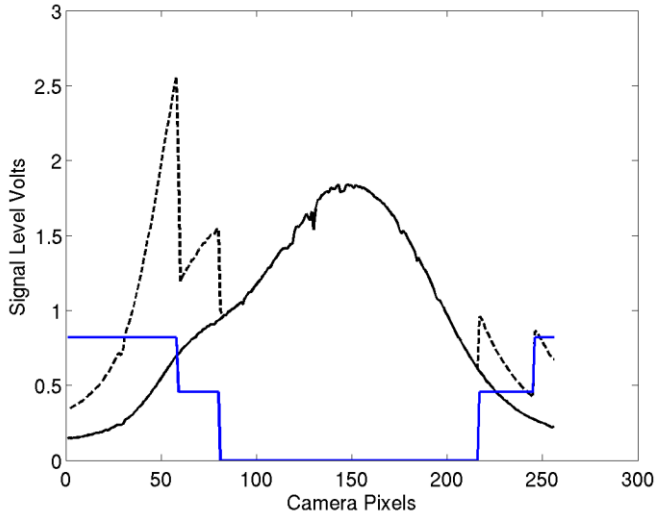

Figure 8 - DC levels on the detector with different gains.

REFERENCES

1. Yadid-Pecht, O., and Fossum, E., "Wide intrascene dynamic range CMOS APS using dual sampling," IEEE Transactions on Electron Devices 44(10), 1721-1723 (1997).
2. Hosticka, B., Brockherde, W., Bussmann, A., Heimann, T., Jeremias, R., Kemna, A., Nitta, C., and Schrey, O., "CMOS imaging for automotive applications," IEEE Transactions on Electron Devices 50(1), 173-183 (2003).
3. Ide, N., Lee, W., Akahane, N., and Sugawa, S., "A Wide DR and Linear Response CMOS Image Sensor with Three Photocurrent Integrations in Photodiodes, Lateral Overflow Capacitors, and Column Capacitors," IEEE Journal of Solid-State Circuits 43(7), 1577-1587 (2008).
4. Cheng, H., Choubey, B., and Collins, S., "An Integrating Wide Dynamic-Range Image Sensor with a Logarithmic Response," IEEE Transactions on Electron Devices 56(11), 2423-2428 (2009).
5. Guo, J., and Sonkusale, S., "An auto-switched mode CMOS image sensor for high dynamic range scientific imaging applications," in IEEE Sensors 2008, 355-358 (2008).
6. Boulade, O., Charlot, X., Abbon, P., Aune, S., Borgeaud, P., Carton, P., Carty, M., Da Costa, J., Deschamps, H., et al., "MegaCam: the new Canada-France-Hawaii Telescope wide-field imaging camera," in Instrument Design and Performance for Optical/Infrared Ground-based Telescopes 4841, 72-81 (2003).
7. Holland, S., Bebek, C., Daniels, P., Dawson, K., Ernes, J., Groom, D., Jelinksy, S., Karcher, A., Kolbe, W., et al., "Technology development for 4k × 4k, back-illuminated, fully depleted scientific CCD imagers," in Nuclear Science Symposium Conference Record 2007 2220-2225 (2007).
8. Mosconi, D., Stoppa, D., Malfatti, M., Perenzoni, M., Scandiuzzo, M., and Gonzo, L., "A CMOS Sensor based on Single Photon Avalanche Diode for Fluorescence Lifetime Measurements," in Instrumentation and Measurement Technology Conference, 2006 416-419 (2006).
9. Niclass, C., Favi, C., Kluter, T., Gersbach, M., and Charbon, E., "A 128 × 128 Single-Photon Image Sensor With Column-Level 10-Bit Time-to-Digital Converter Array," IEEE Journal of Solid-State Circuits 43(12), 2977-2989 (2008).
10. Smith, R.J., Somekh, M.G., Sharples, S.D., Pitter, M., Light, R.A., and Johnston, N., "Parallel Detection in Picosecond Ultrasonics with both Commercial and Custom Array Detection," in 1st Symposium of Laser Ultrasonics (2008).
11. Spirig, T., Seitz, P., Vietze, O., and Heitger, F., "The lock-in CCD-two-dimensional synchronous detection of light," IEEE Journal of Quantum Electronics 31(9), 1705-1708 (1995).

12. Oike, Y., Ikeda, M., and Asada, K., "High-performance photo detector for correlative feeble lighting using pixel-parallel sensing," IEEE Sensors Journal 3(5), 640-645 (2003).
13. Bourquin, S., Seitz, P., and Salathe, R., "Two-dimensional smart detector array for interferometric applications," Electronics Letters 37(15), 975-976 (2001).
14. Ando, S., and Kimachi, A., "Correlation image sensor: two-dimensional matched detection of amplitude-modulated light," IEEE Transactions on Electron Devices 50(10), 2059-2066 (2003).
15. Pitter, M., Light, R., Somekh, M., Clark, M., and Hayes-Gill, B., "Dual-phase synchronous light detection with 64×64 CMOS modulated light camera," Electronics Letters 40(22), 1404-1405 (2004).
16. Johnston, N., Stewart, C., Light, R., Hayes-Gill, B., Somekh, M., Morgan, S., Sambles, J., and Pitter, M., "Quad-phase synchronous light detection with 64 X 64 CMOS modulated light camera," Electronics Letters 45(21), 1090-1091 (2009).
17. Wright, O.B., Hyoguchi, T., and Kawashima, K., "Laser Picosecond Acoustics in Thin Films: Effect of Elastic Boundary Conditions on Pulse Generation," Japanese Journal of Applied Physics 30, L131-L133 (1991).
18. Thomsen, C., Grahn, H., Maris, H., and Tauc, J., "Picosecond interferometric technique for study of phonons in the brillouin frequency range," Optics Communications 60(1-2), 55-58 (1986).